

# Somatosensory Organ Topography Across the Star of the Star-Nosed Mole (*Condylura cristata*)

Eva K. Sawyer<sup>1\*</sup> and Kenneth C. Catania<sup>2</sup>

<sup>1</sup>Neuroscience Graduate Program, Vanderbilt University, Nashville, Tennessee 37240

<sup>2</sup>Department of Biological Science, Vanderbilt University, Nashville, Tennessee 37232

## ABSTRACT

Quantifying somatosensory receptor distribution in glabrous skin is usually difficult because of the diversity of skin receptor subtypes and their location within the dermis and epidermis. However, the glabrous noses of moles are an exception. In most species of moles, the skin on the nose is covered with domed mechanosensory units known as an Eimer's organs. Eimer's organs contain a stereotyped array of different mechanosensory neurons, meaning that the distribution of mechanosensitive nerve endings can be inferred by visual inspection of the skin surface. Here we detail the distribution of Eimer's organs on the highly derived somatosensory star on the rostrum of the star-nosed mole (*Condylura cristata*). The star con-

sists of 22 fleshy appendages, or rays, that are covered in Eimer's organs. We find that the density of Eimer's organs increases from proximal to distal locations along the length of the star's rays with a ratio of 1:2.3:3.1 from the surface nearest to the nostril, to the middle part of ray, to the ray tip, respectively. This ratio is comparable to the increase in receptor unit density reported for the human hand, from the palm, to the middle of the digits, to the distal fingertips. We also note that the tactile fovea of the star-nosed mole, located on the medial ventral ray, does not have increased sensory organ density, and we describe these findings in comparison with other sensory fovea. *J. Comp. Neurol.* 524:917–929, 2016.

© 2015 Wiley Periodicals, Inc.

**INDEXING TERMS:** sensory system; touch; receptor topography; RRID:nif-0000-30467; RRID:rid\_000042

Investigations of somatosensory receptor arrangement in most skin surfaces require multiple visualization techniques and must account for distortions caused by cutting and staining tissue (Miller et al., 1958; Novotny and Gommert-Novotny, 1988; Nolano et al., 2003; Li et al., 2011). Because quantifying skin somatosensory receptors is difficult, efforts to describe the topography of mechanoreceptor distribution lag behind similar observations in the visual system, where flattened retinal preparations have been used to determine photoreceptor distribution (Curcio et al., 1987, 1990; Packer et al., 1989). Unlike the mechanoreceptors that densely innervate the fingertips, lips, and oral cavity of many vertebrates (Dixon, 1961; Halata and Munger, 1983; Pare et al., 2002), the somatosensory Eimer's organs (EOs) of the mole display distinctive morphology that is readily visible on the superficial sensory epithelium. The superficial shape of EOs on the glabrous rostrum of moles provides an opportunity to map sensory units on a tactile surface to a level of detail comparable to that of flattened retinal preparations.

EOs are domed papillae that house clusters of multiple mechanosensory cell types (Eimer, 1871). These organs are present on the nose of most members of the mole fam-

ily (Talpidae; Catania, 2000). However, star-nosed moles (*Condylura cristata*; Fig. 1A) have the greatest number of EOs, and individual EOs in this species are smaller in diameter than those of other species (Catania, 1995a). These EOs cover the entire surface of the star, which is composed of 22 extensions, or rays (see Fig. 1B for the ray numbering convention). EOs consist of a stereotyped arrangement of at least four kinds of mechanoreceptor endings, including a laminated corpuscle, a Merkel cell-neurite complex, a class of presumptive light-touch-mediating free nerve endings, and a class of presumptive nociceptive free nerve endings (Marasco et al., 2006). The

Grant sponsor: National Institutes of Health; Grant number: NS084706 (to E.K.S.); Grant number: National Science Foundation; Grant number: 1456472 (to K.C.C.).

Grant sponsor: National Institutes of Health; Grant number: NS084706; Grant sponsor: National Science Foundation; Grant number: 1456472.

\*CORRESPONDENCE TO: Eva Sawyer, Department of Psychology, Vanderbilt University, PMB 407817, 2301 Vanderbilt Place. Nashville, TN 37240-7817. E-mail: eva.k.sawyer@vanderbilt.edu

Received September 10, 2015; Revised November 20, 2015; Accepted November 23, 2015.

DOI 10.1002/cne.23943

Published online December 29, 2015 in Wiley Online Library (wileyonlinelibrary.com)

© 2015 Wiley Periodicals, Inc.

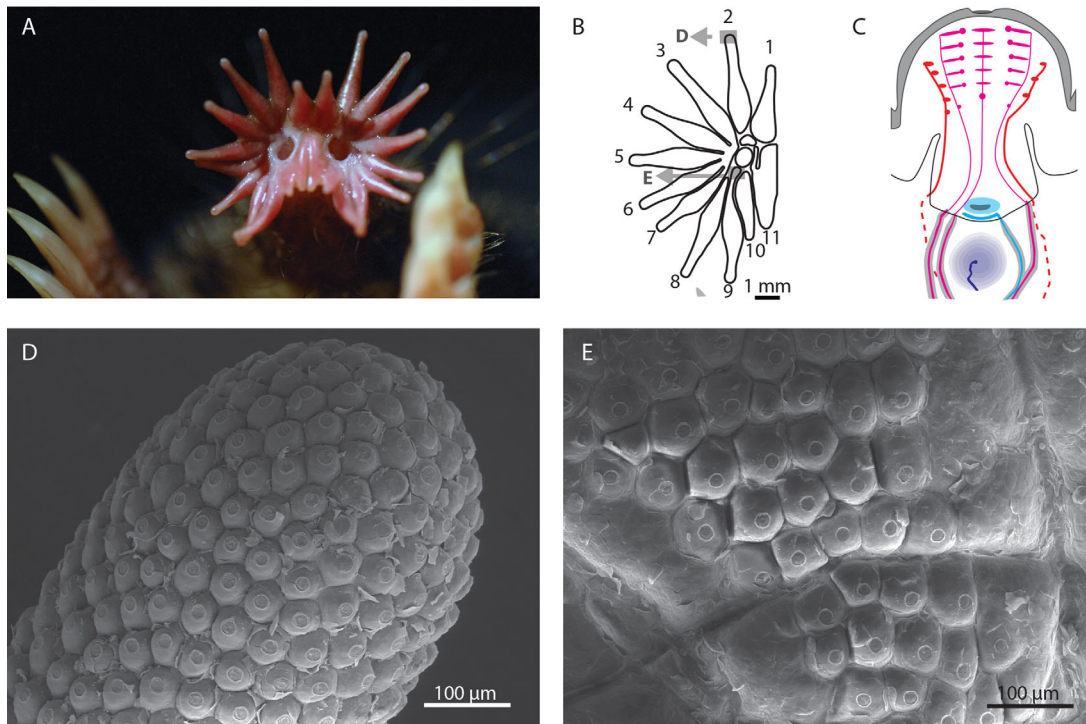


**Figure 1.** Somatosensory surface of the star of a star-nosed mole (*Condylura cristata*). **A:** Star of a star-nosed mole. **B:** Schematic of the star. At left, the rays are numbered according to the conventional numbering system. Small gray rectangles show the locations of D and E. **C:** Schematic of the dermal innervation of an Eimer's organ, the repeated somatosensory unit on the star based on Catania (1995c). Each EO has one laminated corpuscle (dark blue) and one Merkel cell–neurite complex (light blue). The free nerve endings are pink and red. There are seven or eight presumptive light-touch-mediating fibers (pink) and an unquantified number of presumptive pain-mediating fibers (red). **D,E:** Scanning electron micrographs from the tip of a ray and the base of a ray, respectively. Scale bars = 1 mm in B; 100  $\mu\text{m}$  in D,E.

cellular anatomy of an EO of a star-nosed mole is shown in Figure 1C (Catania, 1995c, 1996). Externally, each EO of a star-nosed mole appears as a raised papilla with a dimple in the center (Fig. 1D,E). The highly specialized rostrum of the star-nosed mole is covered in these papillae, making this skin surface a star-shaped sheet of discrete somatosensory organs.

The star of the star-nosed mole is additionally noteworthy for the special properties of ray 11, the medial ventral ray. There is a behavioral preference to use this ray. For example when another part of the star touches a potential food item, the mole reorients its head and star so that ray 11 makes contact with the item prior to ingestion (Catania and Remple, 2004). Furthermore, the extensive use of ray 11 is reflected in the central nervous system, where, despite the small surface area of the ray, its representation takes up 25% of the total star representation in primary somatosensory cortex (Catania, 1995b; Catania and Kaas, 1997). In addition, cortical multiunit receptive fields are smaller on ray 11 than on other rays (0.58  $\text{mm}^2$  on ray 11 compared with 0.82  $\text{mm}^2$  on the other rays), implying a difference in tactile resolution

(Sachdev and Catania, 2002). For these reasons, ray 11 has been called a “somatosensory fovea.”

Sensory foveae have been described in other sensory systems. Often they are marked by a higher density of sensory receptors compared with contiguous sensory surfaces (Pettigrew and Frost, 1985; Bacelo et al., 2008), yet no specialization in the arrangement of EOs has been found for ray 11 in star-nosed moles.

Variation in the size and density of EOs in the star-nosed mole has been previously noted but not thoroughly quantified (Van Vleck, 1965; Catania, 1995c). More specifically, the EOs on the tips of the rays were reported to be smaller and more densely packed than those at the base of the rays (Fig. 1C–E), and EOs on ray 11 have a density similar to that on other rays (Van Vleck, 1965; Catania, 1995c). Here we quantify the distribution of EOs on the forward-facing star surface to test these observations further. We chose to focus on only the rostral surface of the star (although EO's ring the distal portion of most rays) because the front of the star is the part that comes into most frequent contact with the substrate as the mole explores its environment (Catania and Remple, 2004). Also, the rostral surface of the star is where the

majority of receptive fields were found and measured during electrophysiological recordings in somatosensory areas in the brainstem and cortex (Catania and Kaas, 1995; Catania et al., 2011; Sawyer et al., 2014). Our goals were to document the receptor distribution to a level not possible for other glabrous skin surfaces and to determine whether the distribution of EOs on ray 11 differed from that of the other rays.

## MATERIALS AND METHODS

### Animals

No animals were killed for this project. Star skin surfaces were obtained from stored samples from adult star-nosed mole (*Condylura cristata*) that had been killed for other research projects. Those projects conformed to the National Institutes of Health standards concerning the use and welfare of experimental animals and were approved by the Vanderbilt University Animal Care and Use Committee (Animal Welfare Assurance No. A-3227-01).

Stars with obvious scars and abrasions indicating natural use-dependent injury/damage were excluded. Fifteen stars were used in total. These were all from adult individuals that had been collected in Potter County, Pennsylvania (Pennsylvania Game Commission permit 112-2011). Moles had been killed with an overdose of sodium pentobarbital (120 mg/kg) and transcardially perfused with phosphate-buffered saline (pH 7.3) followed by 4% paraformaldehyde. The star had been removed and placed in 4% paraformaldehyde for at least 2 months before being retrieved for use in this project.

### Whole-star measurements

For all samples, stars were rinsed in PBS, and the muscle tissue around the star was trimmed away to leave only the glabrous star skin surface. For measurements of the shape and sizes of the rays, the star was placed on a light box and under glass slides to press the star flat gently. A photograph of the star and a scale bar was taken from directly above the star with an Olympus TG-2 camera.

### Scanning electron microscopy

Four stars were again rinsed in PBS, trimmed, and gently pressed flat. The sample was then dehydrated in an ethanol series (50%, 70%, 95%, and 100%), critical-point dried in an E3000 drier (Quorum Technologies, Guelph, Ontario, Canada), and coated with gold in a Cressington 108 sputter coater (Cressington Scientific Instruments, Ltd., Watford, United Kingdom). Specimens were imaged in a Tescan Vega II scanning electron microscope (Tescan USA, Cranberry Twp., PA).

### Image analysis

For measurements of the size and shapes of rays, the images were imported into Adobe Illustrator (ver. 17), and the rays were outlined with the pen tool. Rays were numbered as shown in Figure 1C. The outline of the ray was defined at the medial end as areas where there was a break in the receptor sheet or the where receptor sheet of one ray merged with another ray. Tissue with EOs was more opaque than areas where there were breaks in the receptor sheet, making the breaks visible as brighter areas when the star was illuminated from behind.

The image was imported into ImageJ (RRID:nif-0000-30467) and scaled to fit the scale in the image (Schneider et al., 2012). The rays were measured for area and circularity using the Analyze particles function. Circularity, defined as  $4\pi \times \text{area}/\text{perimeter}^2$ , is a dimensionless value that describes how circular a shape is (Russ and DeHoff, 2000). A value of one indicates a perfect circle, whereas a value closer to zero indicates a more elongated shape. Circularity is used to describe biological shapes from neurons to maple leaves (Majumdar and Mallick, 2005; Royer et al., 2009).

The photography, outlining, and measurement of one half star was repeated three times. The coefficient of variation was 3.5% for area measurements and 2.5% for circularity calculations. For five stars, both the left and the right sides were measured, but no laterality effect was detected, so only one side of the remaining stars was measured.

For four stars, SEM photomicrographs were analyzed for measurements of individual organs. In these preparations, only those organs on the forward face of the star and that were completely visible (judged by seeing the outline of the entire organ) were measured. Organs were defined as domes that contained the distinctive round dimple, indicating the mechanosensory column (Catania, 1995c). All of the EOs on five rays were marked three times, and the coefficient of variation for the total number of EOs marked was 1.5%, indicating that we were consistently selecting the same EOs as being on the forward face of the star. The surface area of each EO on two half stars and the density of EO for four whole stars was measured.

To measure surface area, the SEM images were imported into Adobe Illustrator, and EOs were outlined with the pen tool. The image of all the outlined rays was then imported into ImageJ. The image was rotated so that the long axis of the ray was vertical, and only the y coordinate of the EOs was used for analysis. The area of each EO and its y coordinate along the ray was found with the Analyze particles function. The y coordinate was used to calculate "eccentricity," which we defined here as the

**TABLE 1.**  
**Area and Shape of the Surface of Nasal Rays of the Star-Nosed Mole<sup>1</sup>**

Ray		Area (mm <sup>2</sup> )	Percentage of total star area	Circularity
1	Mean (SD)	2.61 (0.4)	9.95 (0.54)	0.48 (0.03)
	Coefficient of variation	15.33	5.43	
2	Mean (SD)	2.93 (0.48)	11.15 (0.82)	0.29 (0.02)
	Coefficient of variation	16.38	7.35	
3	Mean (SD)	2.91 (0.54)	11.05 (0.77)	0.31 (0.02)
	Coefficient of variation	18.56	6.97	
4	Mean (SD)	2.74 (0.43)	10.43 (0.55)	0.32 (0.02)
	Coefficient of variation	15.69	5.27	
5	Mean (SD)	2.34 (0.45)	8.87 (0.70)	0.32 (0.02)
	Coefficient of variation	19.23	7.89	
6	Mean (SD)	2.09 (0.39)	7.93 (0.68)	0.31 (0.02)
	Coefficient of variation	18.66	8.58	
7	Mean (SD)	2.00 (0.36)	7.58 (0.64)	0.31 (0.01)
	Coefficient of variation	18.00	8.44	
8	Mean (SD)	2.55 (0.42)	9.69 (0.50)	0.28 (0.02)
	Coefficient of variation	16.47	5.02	
9	Mean (SD)	2.2 (0.47)	8.32 (1.12)	0.28 (0.03)
	Coefficient of variation	21.36	13.46	
10	Mean (SD)	1.52 (0.24)	5.79 (0.57)	0.43 (0.05)
	Coefficient of variation	15.79	9.84	
11	Mean (SD)	2.4 (0.36)	9.18 (0.74)	0.44 (0.03)
	Coefficient of variation	15.00	8.06	
Total	Mean (SD)	26.29 (4.1)		
	Coefficient of variation	15.60		

<sup>1</sup>The area and shape of the surface of rays on one half of a star (six right, five left). The average value is given with standard deviation in the parentheses. Circularity describes how like a circle the shape is. A value of one indicates a perfect circle, whereas a value closer to zero indicates a more elongated shape. The equation for circularity is: circularity =  $4\pi \times \text{area}/\text{perimeter}^2$ .

distance from the most medial EO on the ray. Percentage eccentricity was found for each ray with the following formula: percentage eccentricity =  $100 \times (\text{distance from base}/\text{length of ray})$ . Percentage eccentricity facilitated comparisons between rays of different lengths.

To measure the density of EOs, SEM images were imported into Adobe Illustrator, and a single dot was placed on the central disk-shaped region of every completely visible individual EO. The image of the dots was then imported into ImageJ. Heat density maps were created in ImageJ by importing this image, using a mean filter, and then implementing the Look Up Table feature for coloring. The raw image was also further analyzed for the density measurements used in the statistical analyses. For this, every EO not on a ray was placed in the "center" group. For every EO on a ray, the rays were divided into 20 sections with approximately equal numbers of EOs in each section. Each section was outlined and the area of each section found in ImageJ. The density was calculated as the number of EOs in that portion of the star divided by the area. Statistical analysis was performed in SPSS ver. 22 (RRID:rid\_000042).

## RESULTS

The areas of the rostral star surface varied between individuals, but the relative sizes of this surface of each

ray on their stars were consistent. Ray 10 had the smallest surface area, and many rays were grouped as having similarly large surface areas. Rays 2, 8, and 9 were the most elongated (most eccentric), and ray 1 was the most circular (least eccentric). EOs covered the star in a hexagonal array. EOs were larger and less densely packed toward the base of the rays than toward the tips.

### Size and shape of the star

The area and circularity of the frontal surface area of the rays are shown in Table 1 and Figure 2. A one-way ANOVA revealed that there was an effect of ray on rostral surface area of the star ( $F_{10,110} = 11.259$ ,  $P < 0.01$ ). A post hoc Tukey's HSD revealed that ray 10 had the smallest surface area. The test grouped rays 1, 2, 3, 4, 8, and 11 as having the largest rostral surface area. The rostral surface area of a ray was related to the rostral surface area of the other rays on the star (e.g., a large ray 1 was from a star that also had large rays 2–11). This relationship was seen in that the area of each ray was positively related to the overall size of the rest of the star (e.g., the sum of the areas of the other 10 rays) so that  $P < 0.01$  for all 11 linear regressions. The coefficient of variation for individual rays, which represents within-species variation, was between 15.0% and 21.4% and was 15.6% for the overall size of the star. The body mass and length of

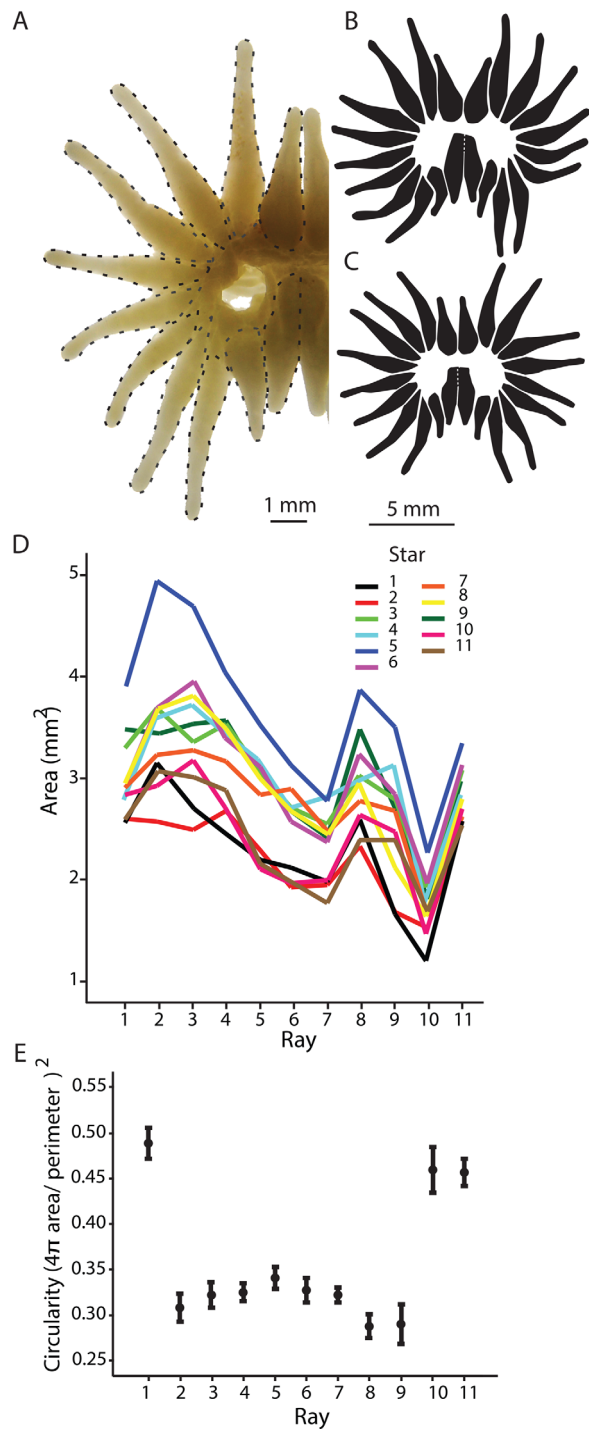


**Figure 2.** Shape and size of the rays. **A:** Example image showing the definitions of the rays. **B,C:** Two images of traced stars shown as example results. **D:** Graph of the frontal surface area of individual rays from 11 different arrays of stars. **E:** Graph of the average circularity measurements of the frontal surface of individual rays from 11 stars. The bars indicate 95% confidence intervals. Scale bars = 1 mm in A; 5 mm in B,C.

the individual animals from which the stars originated were unknown, so no further analysis of how stars varied with body size could be completed.

Ray number also had a significant effect on circularity (ANOVA  $df = 10$ ,  $F = 108.458$ ,  $P < 0.0001$ ). Ray 1 was the most circular, followed by rays 10 and 11. Not captured in these measurements is that the receptor sheet is continuous from ray 11 on one side and its contralateral counterpart. This is not the case for ray 1, the other midline ray. Rays 8, 9, and 2 had the most elongated shapes.

### Density of EOs

In the four complete stars analyzed for EO density, EOs were most tightly packed at the tips of the rays and were less dense at the base of the rays and near the nostril (Fig. 3A,C,E,G). When the density of EOs was plotted against the percentage eccentricity, the curve of every ray on each star fit both a linear function and a cubic function ( $P < 0.01$ ). The R-squared for the linear equations was between 0.21 and 0.82 and for the cubic equations between 0.51 and 0.90. In all cases the value of R-squared for the cubic function was greater than the value of R-squared for the linear functions. The cubic function described a curve in which EO density was lowest at the base of the ray and increased to an eccentricity of approximately 25% (Fig. 3B,D,F,H). The density then plateaued until increasing again in the most distal 10% of the ray. The shape of the curve was used as a guide to group the measurements of density into three parts on the ray and the base area near the nostrils. Pooling all stars and rays, the average density and standard deviation were  $228.35 \pm 45.6$  EO/mm<sup>2</sup> for the center of the star,  $390.7 \pm 74.6$  EO/mm<sup>2</sup> for the base of the ray,  $515.6 \pm 84.7$  EO/mm<sup>2</sup> for the middle portion of the ray, and  $718.0 \pm 106.3$  EO/mm<sup>2</sup> for tip of the ray. Following these subdivisions, the ratio of densities for EOs at the center portion of the star (not on a ray), to the base of a ray (0–25% eccentricity), to the middle portion of the star (25–85% eccentricity), to the tip of the ray (85–100% eccentricity) was 1:1.3:2.6:3.1.

Those groupings were used when comparing the density of the organs on different rays. A one-way ANOVA for EO density with ray as a factor showed no difference in the density of the rays when grouped by ray base, middle, and tip. There was no difference between rays when the areas were pooled. The average number of EOs on the surface of the rays was  $8,169 \pm 414$ .

### Size of EOs

The trends for EO size mirrored the findings for density. In all rays, EOs were largest at the base of the rays, appeared moderately sized throughout the middle half of the ray, then smallest at the tip of the ray (Fig. 4, Table 2). The histograms in Figure 4B and D show the frequencies of the area measurements of EOs in

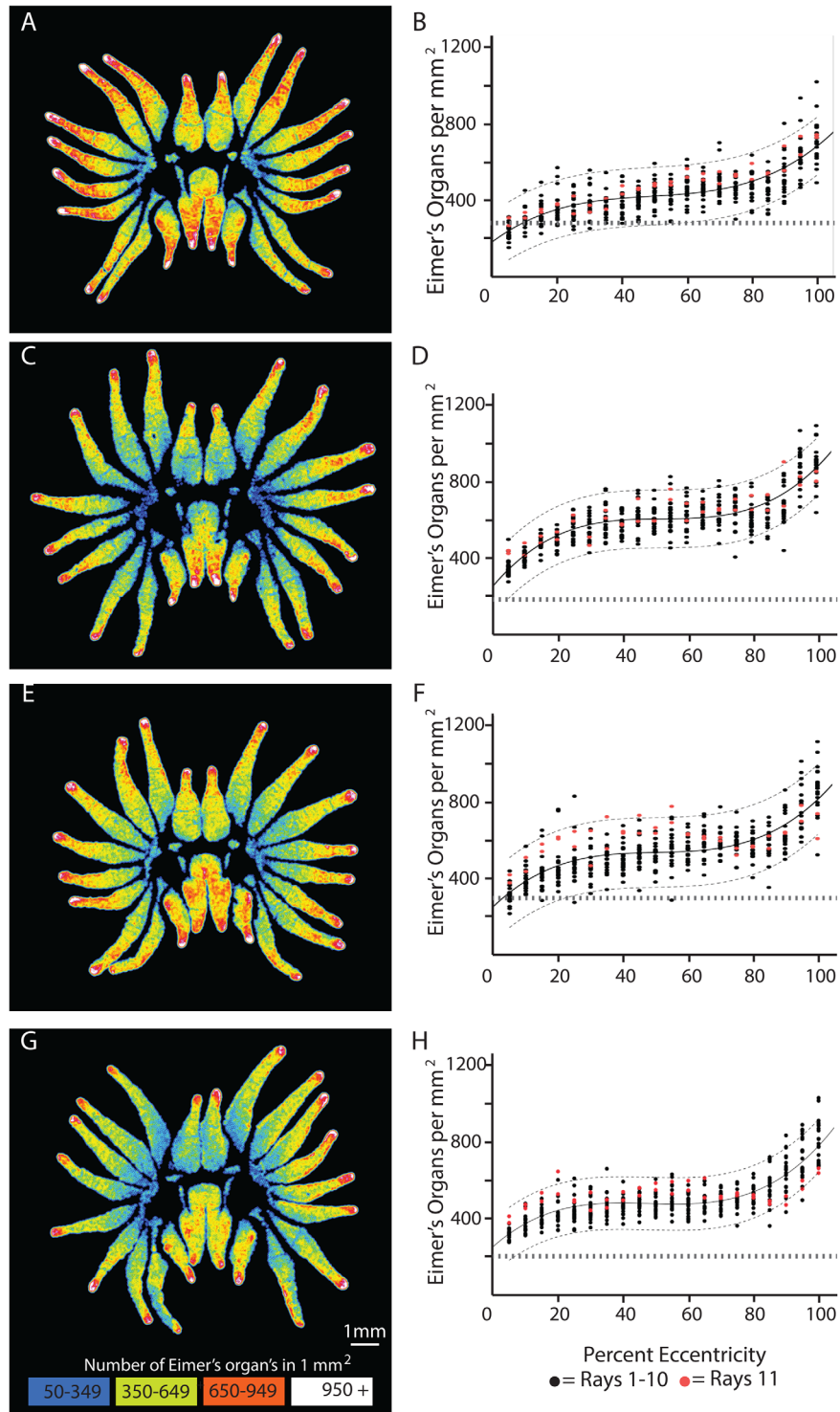


**Figure 3.** Density of EOs on the star surface. **A,C,E,G:** Colored heat maps of the density of EOs on the flattened surface of four stars for stars A–D, respectively. **B,D,F,H:** Density of EOs plotted against the normalized distance from the base of the ray for stars A–D, respectively. Percent eccentricity =  $100 \times (\text{distance from base}/\text{length of ray})$ . Solid lines are the best-fit cubic equation for all rays. Black dashed lines are 95% confidence interval around the best-fit curve, and the gray dotted lines are the average density of the EOs on the base portion of the star around the nostrils. The density of organs on the somatosensory fovea, ray 11, is similar to that of other rays. Scale bar = 1 mm.

the center portion of the star, in rays 1–10, or in ray 11. The histograms show that 1) the sizes of EO on the rays fall into a slightly right-shifted distribution; 2)

within a star, the distribution of sizes is similar between ray 11 and all the other rays, 3) the size of the EOs not on a ray is not right shifted, and 4) EOs on star A had

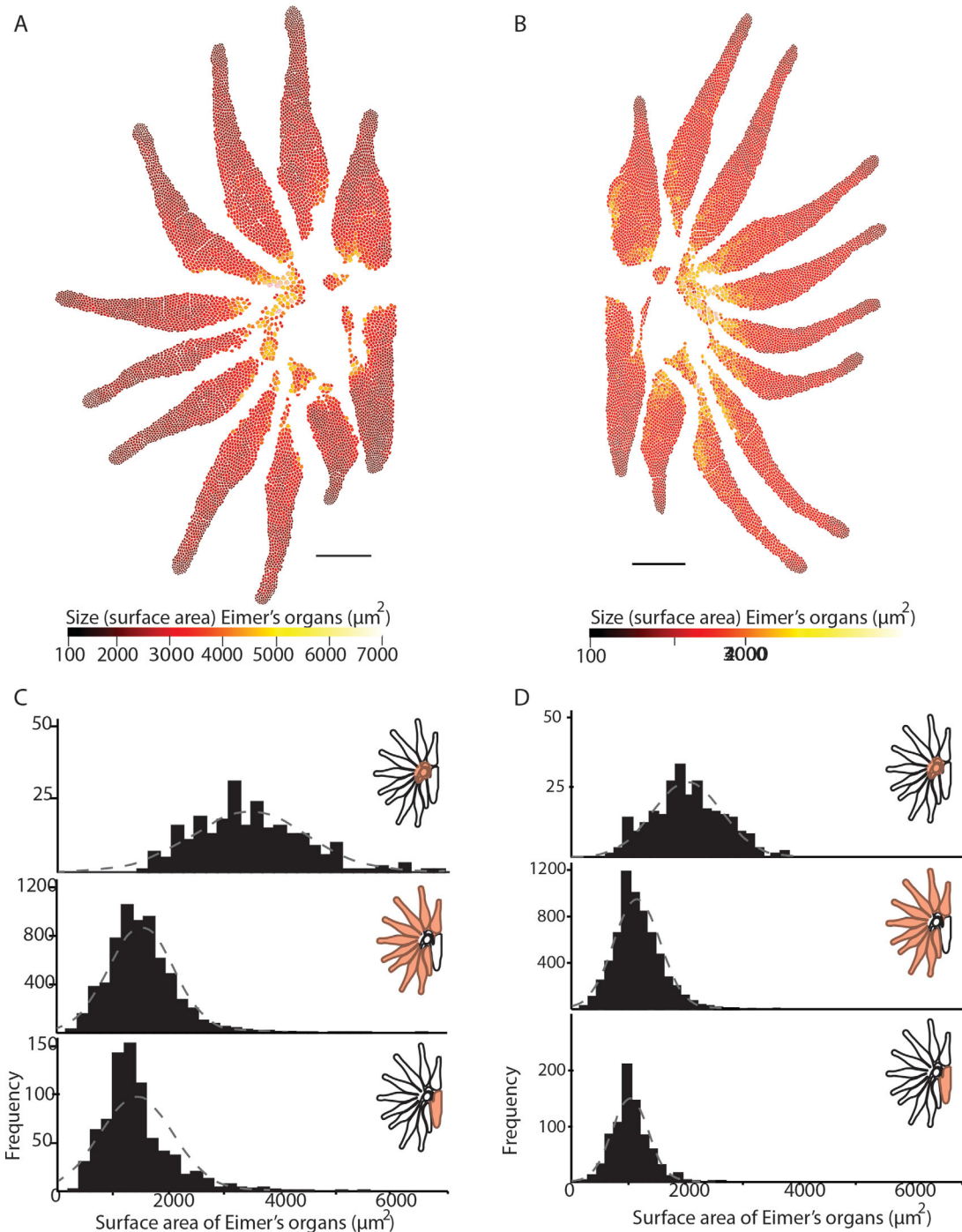


**Figure 4.** Surface area of the EOs on the flattened surface of a sensory star. **A,B:** One half of the sensory star from cases A and B, respectively. The size of the EO is represented with color, as shown in the key below each image. **C,D:** Histograms displaying the frequency of EOs with different surface areas in stars A and B, respectively. In each column the topmost histogram displays the results for the base area of the star, the middle histogram for rays 1–10, and the bottom histogram for ray 11. The dotted line shows a normal distribution. Scale bars = 1 mm.

a greater range of sizes than EOs on star B. Some of this variation could be due to differences in tissue shrinkage during preparation for SEM.

In all rays, the relationship between eccentricity and surface area of the EOs was well described by a linear

function ( $P < 0.01$  for all linear regressions, R-squared values ranging from 0.42 to 0.78). The shape of the curves again suggested a cubic relationship, which was also tested and found to be significant ( $P < 0.01$  for all cubic regressions, R-squared values ranging from 0.47

**TABLE 2.**  
The Mean Surface Area of Eimer's Organs on the Star of the Star-Nosed Mole<sup>1</sup>

Star	Ray	Base			Middle			Tip			Full ray		
		Mean Area (µm <sup>2</sup> )	N	SD	Mean Area (µm <sup>2</sup> )	N	SD	Mean Area (µm <sup>2</sup> )	N	SD	Mean Area (µm <sup>2</sup> )	N	SD
A	1	2358.37	190	737.72	1662.79	495	441.94	841.57	49	236.43	1788.02	734	656.05
A	2	2166.02	154	553.54	1519.92	641	403.07	676.48	90	184.66	1546.57	885	564.38
A	3	2223.8	192	536.05	1561.01	569	400.57	792.38	72	197.2	1647.34	833	569.09
A	4	2555.13	127	864.91	1473.07	522	399.79	709.58	71	242.59	1588.64	720	709.68
A	5	2357.19	108	657.3	1435.49	467	306.07	826.86	65	179.03	1529.22	640	562.44
A	6	2143.67	70	521.33	1307.67	375	314.15	634.4	65	162.05	1336.6	510	515.58
A	7	2202.81	108	588.89	1327.85	438	384.11	731.9	63	188.66	1421.36	609	578.56
A	8	2286.86	114	465.04	1534.85	462	412.07	748.97	72	259.63	1579.83	648	576.63
A	9	2738.45	40	594.91	1709.96	428	424.33	969.83	65	347.49	1696.88	533	575.57
A	10	1831.74	104	644.18	1448.35	306	420.24	585.1	41	147.7	1458.28	451	564.26
A	11	2138.42	125	632.67	1369.53	588	540.66	673.85	72	174.89	1428.16	785	648.23
A	Center												
A	Full star	2255.04	1332	659.29	1490.51	5291	429.31	744.98	725	238.45	3389.2	255	996.65
B	1	1449.71	217	364.64	1207.31	529	343.28	502.84	49	146.66	1230.05	795	402.49
B	2	1500.63	150	345.08	1102.23	572	273.27	522.53	70	157.8	1126.45	792	371.16
B	3	1439.77	198	277.41	999.45	571	223.61	647.98	60	117.91	1079.18	829	320.42
B	4	1552.98	189	299.23	1086.2	439	242.22	592.45	66	159.58	1166.36	694	374.12
B	5	1620.01	144	408.27	1080.61	417	236.14	581.68	56	155.64	1161.21	617	403.3
B	6	1621.52	104	460.89	992.22	359	208.41	616.1	51	153.37	1082.23	514	401.85
B	7	1803.97	90	336.37	1046.77	328	240.8	524.83	60	148.65	1123.82	478	447.32
B	8	1801.66	91	380.24	1279.5	389	270.05	714.23	70	189.13	1293.95	550	406.77
B	9	1855.83	87	391.44	1321.13	386	320.35	747.85	67	222.96	1336.15	540	436.59
B	10	1768.98	101	361.6	1150.46	382	288.85	477	36	153.96	1224.11	519	434.61
B	11	1359.78	138	263.58	1020.1	605	273.52	582.67	58	120.94	1046.95	801	320.12
B	Center												
B	Full star	1573.41	1509	380.16	1111.34	4977	288.57	599.92	643	179.94	1193.09	7393	434.833

<sup>1</sup>The area, sample size, and standard deviation for Eimer's organs on various parts of the star. The base (percent eccentricity between 0 and 25), middle (percent eccentricity between 25 and 85), and tip (percent eccentricity between 85 and 100) groupings are based on the pattern of density change along the ray.

to 0.79). For each ray, the R-squared values for the cubic functions were always greater than for the linear function.

For star A, the largest EO was 26.6 times larger in area than the smallest; in star B, it was 25.5 times larger in area. However, the variation within 2 standard deviations of the mean was more modest, with EOs at the 97.5th percentile being 6.1 and 4.8 times larger than those at the 2.5 percentile for cases A and B, respectively. Values for the mean size of the EOs on the different regions of the ray (base, middle, and tip as defined above) are shown in Table 2. The maximum size of EOs in case A was larger than that in case B.

## DISCUSSION

Our results take advantage of the punctate distribution of EOs to document the distribution of somatosensory units on a glabrous skin surface with great precision. We show that in the star-nosed mole the area of the dome of an EO usually varies over a factor of approximately 5.5 (but can vary over a larger range), with larger and less densely distributed EOs near the nostrils and smaller more densely distributed EOs near the tips of the rays. The variation of EO size and density could have effects on the sensitivity and resolving power of different portions of the sensory star. However, we found no evidence that the fovea-like properties of ray 11, which include smaller cortical receptive fields and greater cortical magnification in that ray compared with other rays, are related to the density of sensory organs on the star surface.

### Comparison with previous work on the star

Variation in EO density has been recognized in the star surface of the star-nosed mole. Van Vleck (1965) suggested that EOs on the sides of the rays are larger than those on the flat, forward-facing portion of the star. It has also been noted that the EOs at the tips of the rays are smaller in diameter, and thus denser, than those at the base of the rays (Catania, 1995c). Our general findings are that 1) EOs are larger and less dense at the base of the rays than at the tips of the rays and 2) the distribution of EOs on ray 11 appears the same as on other rays are consistent with previous reports (Van Vleck, 1965; Catania, 1995c). The current, more detailed analysis allows for more comprehensive comparisons with other somatosensory sensory epithelia.

A priori mapping of EOs on a star might suggest the distal tips of each ray, with their high density of EOs, as the likely candidate sites for elaborated somatosensation. However, previous behavioral, neuroanatomical, and electrophysiological investigations instead highlight the significance of ray 11 (Catania and Kaas, 1997; Catania

and Remple, 2004). Together these results suggest that the behavioral significance and central nervous system elaboration of ray 11 do not arise solely from the distribution of EOs on the receptor sheet. The results lead to two separate questions. First, why does the fovea not have smaller and denser EOs? Second, why do the tips of the rays have smaller and more dense EOs.

### Why does the fovea not have the highest concentration of EOs?

“Fovea” is Latin for “pit.” This term was employed as an anatomical designation of the dip in the center of the retina, the fovea centralis in primates. The concept of a sensory fovea as a region of a sensory epithelium that is adapted for high spatial resolution has since been expanded and applied to other sensory systems. Outside of the visual system, sensory foveae have been reported for the auditory, somatosensory, and electro-sensory systems (see, e.g., Pettigrew and Frost, 1985; Muller et al., 1992; Iggo et al., 1996; Catania and Kaas, 1997; Covey, 2005; Bacelo et al., 2008; Corfield et al., 2011). Definitions of the term “sensory foveae” vary but usually include at least the following requirements: 1) a higher density of sensory receptors in the foveal area than the surroundings, 2) a specialized (disproportionally large) central representation, and 3) a sensorimotor system that directs the fovea to the stimuli of interest (Pettigrew and Frost, 1985; Bacelo et al., 2008). The extent to which the reported examples of sensory fovea fit all these points varies.

Star-nosed moles clearly meet the second and third criteria (Catania and Kaas, 1997), but, intriguingly, the sensory organs are equally dense on all rays. The acute sensory resolution does not seem to be reflected by sensory organ distribution. This could be an underappreciated phenomenon in biology; identifying other examples would require a level of detailed neuroanatomical and physiological study that is rarely performed for most species but may also be seen in the auditory system of the big brown bat (Casseday and Covey, 1992; Dear et al., 1993; Covey, 2005). In the case of the star-nosed mole, how localized differences in touch acuity can be supported by a sensory surface with a uniform sensory organ density is at least partially explained by the innervation of the star.

Differences in innervation of the rays, not the EO density itself, very likely explain part of the high-resolution properties of ray 11. There is specialization of the sensory array that is not visible from the external surface of the star. This hypothesis is already supported by previous work (Catania and Kaas, 1997). Nerve counts show that ray 11 has a higher ratio of myelinated nerve fibers to EOs in

comparison with other rays, with approximately seven fibers per EO on ray 11 vs. four fibers per EO on the others. This demonstrates that at the level of the primary sensory axons there is less convergence in ray 11 than in the other rays and, hence, an anatomical basis for greater resolution (Catania and Kaas, 1997).

Another reason that EOs might be of similar size on all the rays is that their size might be dictated by a structural constraint of covering the surface of the star and not a functional one. If the size of the EO were purely based on a structural constraint, then we would not expect a difference in the size of EOs on ray 11. This idea is expanded upon in the next section.

Our finding of equal sensory organ density on all the rays does not fit neatly into a broad intramodality, intra-specific definition of a sensory fovea. The example of the star-nosed mole shows that a strict criterion for a sensory fovea to have a higher density of sensory receptors at the foveal region than at other regions of the sensory epithelium could overlook interesting biology. This also highlights the challenges and utility of trying to define analogous specializations across diverse sensory systems and species. Definitions are perhaps most useful when they point out exceptions.

### Why do the tips of the rays have the highest concentration of EOs?

The distribution of EOs seen in the adult may reflect a mechanical constraint. The star is covered in a hexagonal array of EOs. Hexagonal arrays are a common solution to the problem of how to completely cover a surface (Schwann, 1847). The hexagonal pattern naturally arises in proliferating epithelia (Gibson et al., 2006). This conformation has been described for sensory epithelia such as the array of hair cells in a cochlea, the ommatidia of compound eyes, the distribution of rods and cones on the retina, and the distribution of chemosensory cells on the barbels of fish (Kiyohara et al., 2002) as well as for nonsensory surfaces such as the hairs on *Drosophila* wings, honeycombs, and the epidermis of plant leaves (Gibson et al., 2006). The problems of tiling a ray base and a ray tip may call for units of a different size.

Alternatively, it could be that the small organs are an adaptation for sensitivity (not resolution), and are clustered at the tips of the rays because these are areas specialized for highest sensitivity. "Sensory fovea" is a term used for a specialization for high spatial resolution, but there is no term for the area of the sensory epithelium that is optimal for high sensitivity. A dense distribution of sensory cells could be indicative of a specialization for high sensitivity (de Busserolles et al., 2014). This idea is

also supported by the internal structure of EOs. Although the arrangement of mechanoreceptors within an EO is constant across the star (Catania, 1995c), smaller EOs necessarily have less tissue surrounding the sensory nerve endings than larger EOs. This may endow the smaller EOs with better sensitivity to mechanical deformations. If this is the case, then the high density of sensory organs at the tip of the ray could be a specialization for high sensitivity. The high density of EOs at a location other than the high-resolution fovea suggests that observations of nonuniform distribution of mechanoreceptors taken alone are insufficient to distinguish a high-resolution fovea in the somatosensory system.

### Comparison with other sensory surfaces

A star-nosed mole EO is consistently composed of seven or eight presumptive light-touch-mediating free nerve endings, one lamellated corpuscle, one Merkel cell-neurite complex, and an unquantified population of presumptive pain-mediating fibers (Catania, 1995c). The average EO density at the tips of the rays is  $718/\text{mm}^2$  ( $\pm 106.2$ ). Therefore, the distal tip of each ray is predicted to have 718 lamellated corpuscles/ $\text{mm}^2$ , 718 Merkel cells/ $\text{mm}^2$ , and 5,385 presumptive light-touch-mediating free nerve endings/ $\text{mm}^2$ . This estimate for the density of nerve endings is greater than approximations and direct measurements from the vast majority of other vertebrate somatosensory surfaces. For example, it is also far denser than the measured values for mechanoreceptors in the primate hand. The density of Meissner's corpuscles in a macaque fingertip has been estimated at  $57.6/\text{mm}^2$ , Pacinian corpuscles at  $1.2/\text{mm}^2$  (Pare et al., 2002), and free nerve endings at  $50\text{--}57/\text{mm}^2$  (Arthur and Shelley, 1959; Novotny and Gommert-Novotny, 1988). Even the most densely innervated tissue in humans, the cornea, contains only 525 terminals/ $\text{mm}^2$  (He et al., 2010).

One of our findings was that the EOs were most dense at the tips of the rays. A concentration of mechanoreceptors at the distal end of an appendage is also found in other taxa. In echidnas, platypus, crocodylians, and several classes of birds, the tip of the snout or bill has the highest density of somatosensory units (Pettigrew and Frost, 1985; Iggo et al., 1996; Manger and Pettigrew, 1996; Swennen, 2004; Leitch and Catania, 2012; Cunningham et al., 2013). Another relevant comparison is with the digits of the hand. The increase in EO density along a ray is reminiscent of the distribution of mechanoreceptor units in the human hand. The density of mechanoreceptor units in the human hand has been estimated by systematically recording single-unit receptive fields from the median nerve, which showed that the density of low-threshold mechanoreceptor units increases from the

palm to the tip of the finger (Johansson and Vallbo, 1979). There is a slight increase in unit density from the palm to the base of the finger and a sharp increase from the main part of the finger to the tip. The relative density of units in the palm to the main part of the finger and then to the fingertip is 1:1.6:4.2 (Johansson and Vallbo, 1979). This ratio is similar to that found in the current study for the density of EOs near the nostrils, in the middle part of the ray, and in the ray tip of 1:2.3:3.1. In humans, the increase in unit density was attributed almost entirely to an increased density of Meissner's corpuscles at the tips of the fingers, whereas lamellated corpuscles retain a uniform distribution over the hand. In the mole's star, unlike in the primate's hand, lamellated corpuscles are more densely distributed at the tips of the appendages than at the base. The nonuniform distribution and high density of lamellated corpuscles could be related to differences in how moles and humans use their mechanosensory appendages to detect textures. Humans do so by moving their hands across a surface, and moles appear to perform this task by rapidly (up to 13 taps/second) probing surfaces (Catania and Remple, 2004). Finally, the measurements of variation in the star can be compared with those from other species. Variation within a species is important to document because such heterogeneity within a species is the raw material from which natural selection works.

Within the somatosensory system in mammals, measures of variation within a species are limited but include analyses of whisker distributions (Van der Loos et al., 1984; Welker and Van der Loos, 1986; Muchlinski, 2010) and histological studies of primate hands (Kelly et al., 2005). In other mammalian sensory systems, interindividual variation has been documented in the composition of the retina (Packer et al., 1989; Curcio et al., 1990) and the morphology of the semicircular canal (Welker et al., 2009; Billet et al., 2012). In non-mammalian species, there is within-species variation in the distribution of the neuromasts of the lateral line system (Schmitz et al., 2008; Wark and Peichel, 2010), electrosensory pit organs (Peach, 2003), and size and distribution of facets of compound eyes (Spaethe and Chittka, 2003).

Some studies have used high coefficients of variation to suggest that a sensory system is under relaxed selection. The logic for this is that sensory systems that are vital for an animal's survival should be constrained by strong stabilizing selection, although less important sensory systems are free to vary more. For example, measurements of the morphology of the semicircular canals in sloths have coefficients of variation near 15%, which is larger than those of closely related species (Billet et al., 2012). This suggests that vestibular sys-

tem of the ponderous sloth is under less intense stabilizing selection than that of closely related species (Billet et al., 2012). A similar interpretation of relaxed selection was suggested for interindividual variation of 10–20% in the number of ampullary organs in some sharks and rays (Peach, 2003). However, the even greater degree of variation in the density of cones in primate retinas (up to 46% interindividual variation in cone density in the human fovea) has not, to our knowledge, been given an evolutionary explanation (Curcio et al., 1987, 1990; Packer et al., 1989; Song et al., 2011). The inconsistency in interpretations is due partially to a lack of information about what are normal levels of within-species variation for different sensory systems and also is due to the different focuses of the studies. Here we show that the active sensory surface of the star-nosed mole's tactile star varies in surface area by approximately 15% and in number of EOs per star by approximately 5% among adults. A likely explanation is that the somatosensory system is able to accommodate this level of peripheral variation and still produce a highly functioning sensory system; it seems unlikely that the specialized tactile star is under minimal selection pressure. In the future it might be interesting to compare the level of variation found here with that of other somatosensory surfaces.

## CONCLUSIONS

Our results document the distribution of somatosensory organs on a sensory epithelium with great precision. We find that the pattern of sensory organ density varies along the star-nosed moles' star appendages similarly to the organization of somatosensory surfaces and the distribution of specialized tactile organs of other animals, most notably along the fingers of humans. We calculate that the nerve endings in the mole's star are remarkably dense, peaking at approximately 7,180 nerve endings/mm<sup>2</sup>. In addition, we find no direct evidence that the remarkable spatial resolution of the somatosensory fovea is related to the density of EOs, an intriguing finding for behaviorally significant sensory surfaces.

Our finding that the 11th ray of the star-nosed mole does not have a higher concentration of EOs, despite meeting other important qualities of previous definitions of a sensory fovea, is noteworthy. The 11th ray of the star nosed mole is special for its role in high-resolution touch, and in some ways it is like the pit in the center of the primate retina. In other ways, as shown here in the distribution of sensory organs, it is different. Our results show that focusing on sensory organ density alone is insufficient to assess the resolving power of a

somatosensory epithelium. These results may be applicable to other vertebrate skin surfaces.

## ACKNOWLEDGMENTS

We thank Elizabeth Catania and Duncan Leitch for assistance in trapping moles in the field and Jon Kaas and Duncan Leitch for their input in the editing of this manuscript.

## CONFLICT OF INTEREST STATEMENT

The authors declare no conflicts of interest.

## ROLE OF AUTHORS

All authors had full access to all the data in the study and take responsibility for the integrity of the data and the accuracy of the data analysis. Study concept and design: EKS. Acquisition of data: EKS. Analysis and interpretation of data: EKS. Drafting of the manuscript: EKS. Critical revision of the manuscript for important intellectual content: KCC. Statistical analysis: EKS. Obtained funding: EKS, KCC.

## LITERATURE CITED

- Arthur RP, Shelley WB. 1959. The innervation of human epidermis. *J Invest Dermatol* 32:397–411.
- Bacelo J, Engelmann J, Hollmann M, von der Emde G, Grant K. 2008. Functional foveae in an electrosensory system. *J Comp Neurol* 511:342–359.
- Billet G, Hautier L, Asher RJ, Schwarz C, Crumpton N, Martin T, Ruf I. 2012. High morphological variation of vestibular system accompanies slow and infrequent locomotion in three-toed sloths. *Proc R Soc Lond B Biol Sci* 279: 3932–3939.
- Casseday JH, Covey E. 1992. Frequency tuning properties of neurons in the inferior colliculus of an FM bat. *J Comp Neurol* 319:34–50.
- Catania KC. 1995a. A comparison of the Eimer's organs of three North American moles: the hairy-tailed mole (*Parascalops breweri*), the star-nosed mole (*Condylura cristata*), and the eastern mole (*Scalopus aquaticus*). *J Comp Neurol* 354:150–160.
- Catania KC. 1995b. Magnified cortex in star-nosed moles. *Nature* 375:453–454.
- Catania KC. 1995c. Structure and innervation of the sensory organs on the snout of the star-nosed mole. *J Comp Neurol* 351:536–548.
- Catania KC. 1996. Ultrastructure of the Eimer's organ of the star-nosed mole. *J Comp Neurol* 365:343–354.
- Catania KC. 2000. Epidermal sensory organs of moles, shrew moles, and desmans: a study of the family talpidae with comments on the function and evolution of Eimer's organ. *Brain Behav Evol* 56:146–174.
- Catania KC, Kaas JH. 1995. Organization of the somatosensory cortex of the star-nosed mole. *J Comp Neurol* 351: 549–567.
- Catania KC, Kaas JH. 1997. Somatosensory fovea in the star-nosed mole: behavioral use of the star in relation to innervation patterns and cortical representation. *J Comp Neurol* 387:215–233.
- Catania KC, Remple FE. 2004. Tactile foveation in the star-nosed mole. *Brain Behav Evol* 63:1–12.
- Catania KC, Leitch DB, Gauthier D. 2011. A star in the brain-stem reveals the first step of cortical magnification. *PLoS One* 6:e22406.
- Corfield J, Kubke MF, Parsons S, Wild JM, Koppl C. 2011. Evidence for an auditory fovea in the New Zealand kiwi (*Apteryx mantelli*). *PLoS One* 6:e23771.
- Covey E. 2005. Neurobiological specializations in echolocating bats. *Anat Rec A Discov Mol Cell Evol Biol* 287:1103–1116.
- Cunningham SJC, Potter MA, Jensen T. Bill morphology of ibises suggests a remote-tactile sensory system for prey detection. *Auk* 127:308–316.
- Curcio CA, Sloan KR Jr, Packer O, Hendrickson AE, Kalina RE. 1987. Distribution of cones in human and monkey retina: individual variability and radial asymmetry. *Science* 236: 579–582.
- Curcio CA, Sloan KR, Kalina RE, Hendrickson AE. 1990. Human photoreceptor topography. *J Comp Neurol* 292:497–523.
- de Busserolles F, Fitzpatrick JL, Marshall NJ, Collin SP. 2014. The influence of photoreceptor size and distribution on optical sensitivity in the eyes of lanternfishes (Myctophidae). *PLoS One* 9:e99957.
- Dear SP, Fritz J, Haresign T, Ferragamo M, Simmons JA. 1993. Tonotopic and functional organization in the auditory cortex of the big brown bat, *Eptesicus fuscus*. *J Neurophysiol* 70:1988–2009.
- Dixon AD. 1961. Sensory nerve terminations in the oral mucosa. *Arch Oral Biol* 5:105–114.
- Eimer T. 1871. Die Schnauze des Maulwurfs als Tastwerkzeug. *Arch Mikr Anat* 7:181–191.
- Gibson MC, Patel AB, Nagpal R, Perrimon N. 2006. The emergence of geometric order in proliferating metazoan epithelia. *Nature* 442:1038–1041.
- Halata Z, Munger BL. 1983. The sensory innervation of primate facial skin. II. Vermilion border and mucosa of lip. *Brain Res* 286:81–107.
- He J, Bazan NG, Bazan HE. 2010. Mapping the entire human corneal nerve architecture. *Exp Eye Res* 91:513–523.
- Iggo A, Gregory JE, Proske U. 1996. Studies of mechanoreceptors in skin of the snout of the echidna *Tachyglossus aculeatus*. *Somatosens Motor Res* 13:129–138.
- Johansson RS, Vallbo AB. 1979. Tactile sensibility in the human hand: relative and absolute densities of four types of mechanoreceptive units in glabrous skin. *J Physiol* 286:283–300.
- Kelly EJ, Terenghi G, Hazari A, Wiberg M. 2005. Nerve fibre and sensory end organ density in the epidermis and papillary dermis of the human hand. *Br J Plastic Surg* 58: 774–779.
- Kiyohara S, Sakata Y, Yoshitomi T, Tsukahara J. 2002. The “goatee” of goatfish: innervation of taste buds in the barbels and their representation in the brain. *Proc R Soc Lond B Biol Sci* 269:1773–1780.
- Leitch DB, Catania KC. 2012. Structure, innervation and response properties of integumentary sensory organs in crocodylians. *J Exp Biol* 215:4217–4230.
- Li L, Rutlin M, Abaira VE, Cassidy C, Kus L, Gong S, Jankowski MP, Luo W, Heintz N, Koerber HR, Woodbury CJ, Ginty DD. 2011. The functional organization of cutaneous low-threshold mechanosensory neurons. *Cell* 147: 1615–1627.
- Majumdar S, Mallick BN. 2005. Cytomorphometric changes in rat brain neurons after rapid eye movement sleep deprivation. *Neuroscience* 135:679–690.
- Manger PR, Pettigrew JD. 1996. Ultrastructure, number, distribution and innervation of electroreceptors and mechanoreceptors in the bill skin of the platypus, *Ornithorhynchus anatinus*. *Brain Behav Evol* 48:27–54.

- Marasco PD, Tsuruda PR, Bautista DM, Julius D, Catania KC. 2006. Neuroanatomical evidence for segregation of nerve fibers conveying light touch and pain sensation in Eimer's organ of the mole. *Proc Natl Acad Sci U S A* 103:9339–9344.
- Miller MR, Ralston HJ 3rd, Kasahara M. 1958. The pattern of cutaneous innervation of the human hand. *Am J Anat* 102:183–217.
- Muchlinski MN. 2010. A comparative analysis of vibrissa count and infraorbital foramen area in primates and other mammals. *J Hum Evol* 58:447–473.
- Muller M, Laube B, Burda H, Bruns V. 1992. Structure and function of the cochlea in the African mole rat (*Cryptomys hottentotus*): evidence for a low frequency acoustic fovea. *J Comp Physiol A Sens Neural Behav Physiol* 171:469–476.
- Nolano M, Provitera V, Crisci C, Stancanelli A, Wendelschafer-Crabb G, Kennedy WR, Santoro L. 2003. Quantification of myelinated endings and mechanoreceptors in human digital skin. *Ann Neurol* 54:197–205.
- Novotny GE, Gommert-Novotny E. 1988. Intraepidermal nerves in human digital skin. *Cell Tissue Res* 254:111–117.
- Packer O, Hendrickson AE, Curcio CA. 1989. Photoreceptor topography of the retina in the adult pigtail macaque (*Macaca nemestrina*). *J Comp Neurol* 288:165–183.
- Pare M, Smith AM, Rice FL. 2002. Distribution and terminal arborizations of cutaneous mechanoreceptors in the glabrous finger pads of the monkey. *J Comp Neurol* 445:347–359.
- Peach MB. 2003. Inter- and intraspecific variation in the distribution and number of pit organs (free neuromasts) of sharks and rays. *J Morphol* 256:89–102.
- Pettigrew JD, Frost BJ. 1985. A tactile fovea in the Scolopacidae? *Brain Behav Evol* 26:105–195.
- Royer DL, Meyerson LA, Robertson KM, Adams JM. 2009. Phenotypic plasticity of leaf shape along a temperature gradient in *Acer rubrum*. *PLoS One* 4:e7653.
- Russ JC, DeHoff RT. 2000. *Practical stereology*. New York: Kluwer Academic/Plenum. p 381.
- Sachdev RN, Catania KC. 2002. Receptive fields and response properties of neurons in the star-nosed mole's somatosensory fovea. *J Neurophysiol* 87:2602–2611.
- Sawyer EK, Leitch DB, Catania KC. 2014. Organization of the spinal trigeminal nucleus in star-nosed moles. *J Comp Neurol* 522:3335–3350.
- Schmitz A, Bleckmann H, Mogdans J. 2008. Organization of the superficial neuromast system in goldfish, *Carassius auratus*. *J Morphol* 269:751–761.
- Schneider CA, Rasband WS, Eliceiri KW. 2012. NIH Image to ImageJ: 25 years of image analysis. *Nat Methods* 9:671–675.
- Schwann T. 1847. *Microscopical researches into the accordance of structure and growth in animals and plants*. London: Sydenham Society.
- Song H, Chui TY, Zhong Z, Elsner AE, Burns SA. 2011. Variation of cone photoreceptor packing density with retinal eccentricity and age. *Invest Ophthalmol Vis Sci* 52:7376–7384.
- Spaethe J, Chittka L. 2003. Interindividual variation of eye optics and single object resolution in bumblebees. *J Exp Biol* 206:3447–3453.
- Swennen CY. 2004. Notes on feeding structures of the black-faced spoonbill *Platalea minor*. *Ornithol Sci* 3:119–124.
- Van der Loos H, Dorfl J, Welker E. 1984. Variation in pattern of mystacial vibrissae in mice. A quantitative study of ICR stock and several inbred strains. *J Hered* 75:326–336.
- Van Vleck D. 1965. The anatomy of the nasal rays of *Condylura cristata*. *J Mammal* 2:248–253.
- Wark AR, Peichel CL. 2010. Lateral line diversity among ecologically divergent threespine stickleback populations. *J Exp Biol* 213:108–117.
- Welker E, Van der Loos H. 1986. Quantitative correlation between barrel-field size and the sensory innervation of the whiskerpad: a comparative study in six strains of mice bred for different patterns of mystacial vibrissae. *J Neurosci* 6:3355–3373.
- Welker KL, Orkin JD, Ryan TM. 2009. Analysis of intraindividual and intraspecific variation in semicircular canal dimensions using high-resolution x-ray computed tomography. *J Anat* 215:444–451.